ICEM 2002
Brugge 25-26 August

Brushless Electrical Machines with Superconducting Rotors

A. Leão Rodrigues

Department of Electrical Engineering
Faculty of Science and Technology
New University of Lisbon
2825-114 Caparica - PORTUGAL
Fax: +351 21294 8532 Email: leao@uninova.pt

Abstract **- This paper is devoted to the Electrical Machines with inclusion of high temperature superconducting (HTS) elements. Much care must be taken in the design of the HTS machines in order to eliminate mechanical stresses in these fragile materials. Reluctance and hysteresis motors are the best candidates to employ these materials in their construction and different design configurations, giving different torques, are considered. The state of art of four different types of HTS electric machines is presented in the paper. Experimental results obtained from a conventional 2 kW stator with different HTS rotors are displayed and compared.**

1. Introduction

Heike Kammerlingh Onnes, of Leiden University, discovered superconductivity in 1911, when mercury was cooled below 4.2 K. However it wasn't until 1986 when Bednorz and Müller discovered the ceramic superconductors [1], that superconductivity started to have real potential in engineering applications. Theoretical and experimental researches show that the HTS electrical machines possess higher values of specific output power, efficiency and power factor compared with conventional electrical machines [2].

The progress in HTS materials gives a strong impulse for elaborating new layouts of HTS machines [3]. These materials are well suited to applications where weight and size are very crucial

The so-called type-II superconductors usually exist in a mixed state of normal and superconducting regions, called a vortex state where vortices of superconducting currents surrounding cores of normal material [4,5,6]. The most obvious advantage of superconductors is their ability to sustain current densities an order of magnitude greater than copper. However a second advantage, and the property exploited in their use in reluctance and hysteresis machines, is their ability to repel flux, or to act as flux barriers, due to their diamagnetic properties.

The aim of this work is the modelling of different types of reluctance and hysteresis machines, performed using the Finite Element software developed at the Department of Engineering, Oxford University [7,8]. The program calculates the magnetic flux in the machine and the induced current distribution in the superconducting pieces. A comparison of the operation of the machine with and without superconducting materials can be made directly, and conclusions on the optimal machine design are drawn.

2. Meissner Motor

The Meissner Motor is a good example to illustrate the diamagnetic behaviour of the superconductor materials. When a superconductor is placed in a magnetic field it behaves as a flux shield due to the persistent electric currents induced at its surface. In consequence the superconductor experiments a repulsion force from the magnetic field, as shown in figure 1. This phenomenon was discovered in 1932 by Meissner e Ochsenfeld.

After the discovery of HTS materials, a prototype of the

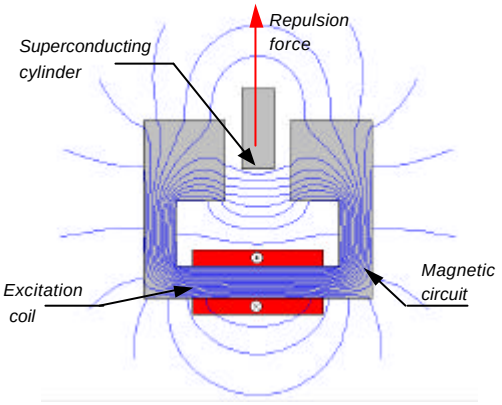

Fig. 1 – Meissner effect

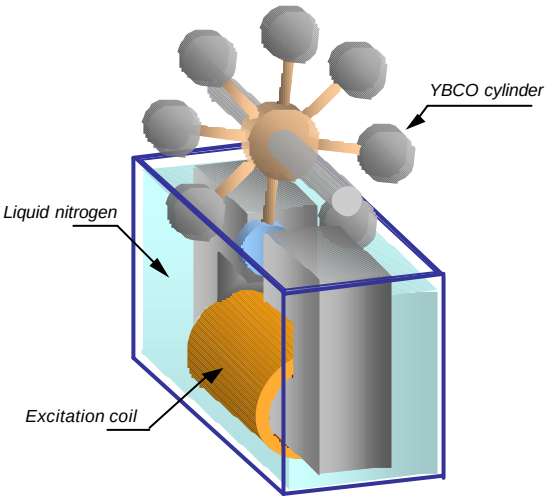

Fig. 2 – Meissner motor

Meissner Motor was constructed in Japan. The rotor consists of a certain number of cylinders of YBCO superconducting material that passes through the air gap of a excited electromagnet bathed by liquid nitrogen, as illustrated in figure 2. The HTS cylinders outside the liquid nitrogen are in normal state and so can easily penetrate inside the air gap. In this region, however, they attain the superconductor state and therefore a repulsion force due to the magnetic field is experimented, generating a torque on the shaft and producing a continuous rotor rotation.
The rotor speed ω of this motor is rather low but the torque T is relatively high, giving a moderate output power $P=T\omega$. This kind of motor illustrates a very unusual approach to the directed energy conversion of the heat energy into the mechanical power one on the base of HTS materials.

3. Salient Type HTS Reluctance Motor

The flux plot of a conventional two pole reluctance motor is shown in figure 3a, where some leakage flux takes place. A low reluctance along the rotor direct axis gives high inductance L_{max} and a high reluctance along the quadrature axis gives a low inductance L_{min} to the stator winding. Assuming sinusoidal variation, figure 3b shows plotted the inductance stator winding variation $L(\theta)$ according to rotor position θ.
The torque produced in a three-phase reluctance motor is given by

$$T(\theta) = \frac{3}{2} I^2 \frac{dL(\theta)}{d\theta} = -\frac{3}{2} I^2 (L_{max} - L_{min}) sen\, 2\theta \qquad (1)$$

and it is shown plotted in figure 3c.
Eq.(1) shows that in order to increase maximum torque the inductance difference (L_{max} -L_{min}) must be improved.

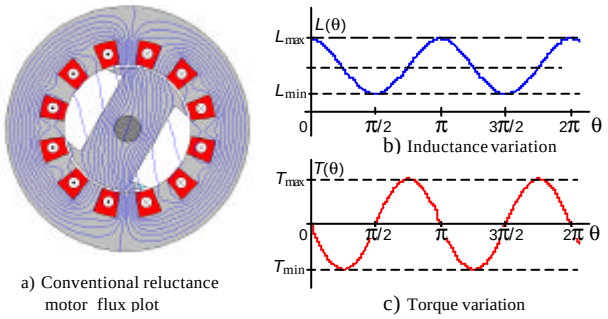

a) Conventional reluctance motor flux plot

b) Inductance variation

c) Torque variation

Fig.3 – Conventional reluctance motor and torque variation

This can be achieved by eliminating rotor leakage flux. Attaching two blocks of HTS flanking the rotor, the difference (L_{max} -L_{min}) is improved since induced currents in the HTS components will prevent flux transverse the quadrature axis and tend to encourage flux along the direct axis. In this scheme shown in figure 4a, HTS blocks work as the concentrators of the magnetic flux along the direct axis.

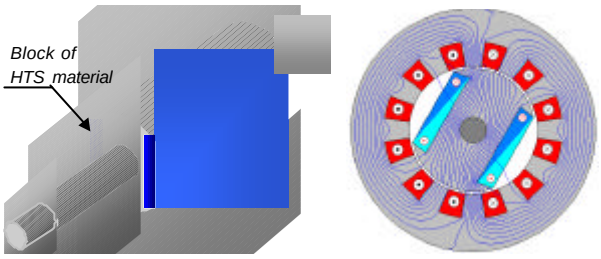

a) Rotor with HTS blocks b) Flux plot

Fig.4 – HTS reluctance motor layout and flux plot

The HTS pieces are electrically separated so that all super current loops must originate and return in the same piece and currents can not transverse the iron. Figure 4b illustrates the flux plot for this new construction where the leakage flux almost disappears. Although this construction is a bit complicated to be constructed the motor has good starting characteristics.

4. "Zebra" Type HTS Reluctance Motor

An interesting alternative to the salient pole machine is the composite or "zebra" motor, that consists of iron segments placed in alternating order with slices of YBCO or Bi-Ag elements, as shown in Figure 5a, and a strong and balanced rotor is obtained.
The operating principle of this motor is similar to the conventional reluctance machine discussed previously. The flux is directed to along the direct axis and a high reluctance value is developed on the quadrature axis. This results in a high value of the difference ($L_{max} - L_{min}$) and according to Eq.(1), a high torque is produced.

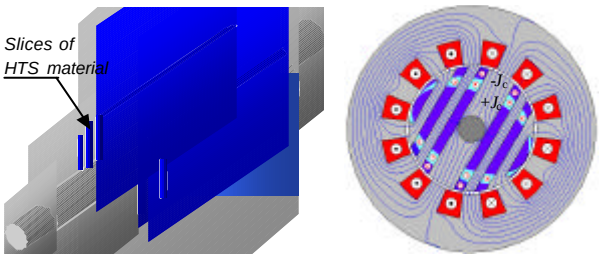

a) Rotor with HTS slices b)Flux plot

Fig.5 – HTS "Zebra" reluctance motor layout and flux plot

Figure 5b shows the flux plot produced by the stator winding in the composite or "Zebra" type rotor. It can be seen that, as in the case of salient type, transport currents $+J_c$ and $-J_c$ are circulating axially in each block, which penetrate about half of the ratio of the rotor [9]. The optimal torque is obtained when the iron and HTS plates have both the same thickness. However, due to the installation of the shaft the middle iron block must be thicker.

5. Novel Synchronous Machine

The longitudinal ends of the two HTS blocks of the reluctance motor can be electrically connected, forming a coil of one single turn, as shown in figure 6a. This allows the pre-magnetisation of the rotor and the machine behaves as a permanent magnet synchronous one [9]. The magnetic flux set up by the pre-magnetised HTS rotor and by stator on load is illustrated in figure 6b.

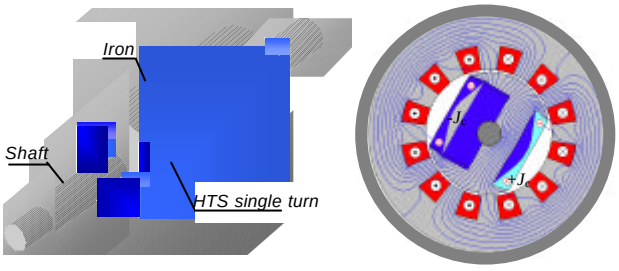

a) Rotor with HTS single turn b)Flux plot

Fig.6 – HTS rotor of a synchronous machine and flux plot

In this case super currents can circulate the iron rotor and forming surrounding loops $+J_c$ and $-J_c$, like a field winding and the rotor behaves as the best-known permanent magnet for the same equivalent volume of the superconductor.
The output torque has now the reluctance component $T_R = A\sin 2\theta$ and an synchronous torque component $T_E = B\sin\theta$, giving a high resulting torque

$$T = A\sin 2\theta + B\sin\theta . \qquad (2)$$

Because the synchronous or excitation torque is usual much greater than reluctance torque, the resulting torque variation has now one cycle per rotor revolution, as shown in figure 7.

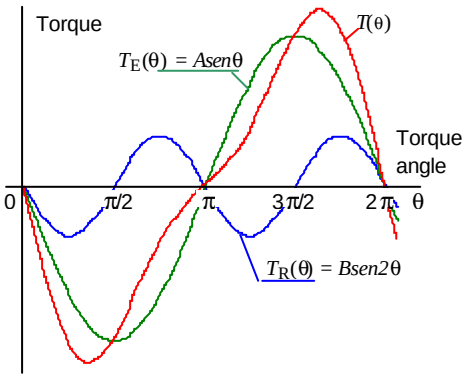

Fig.7 – Torque variation of a salient pole synchronous motor

The stator winding can be used to pre-magnetise the superconductor by field cooling. It is important that the pre-magnetising field penetrates further than the rotating field, otherwise, during the normal operation the trapped field can be lost. The sequence of the HTS coil pre-magnetisation is illustrated in figure 8. With the ceramic material in the normal state, $T > T_c$, a static stator field is switched on. A flux density of about twice of the flux during normal operation is desirable. The second step is to cool the HTS rotor with liquid nitrogen at temperature $T < T_c$ and maintaining the stator field. In this situation the HTS material attains the superconducting state by field cooling. Finally, the stator current is switched off and super currents are induced in the superconductor penetrating further in the material. Therefore the rotor retains some trapped flux behaving as a permanent magnet. The situation is maintained while the HTS material of the rotor is kept with a temperature $T < T_c$.

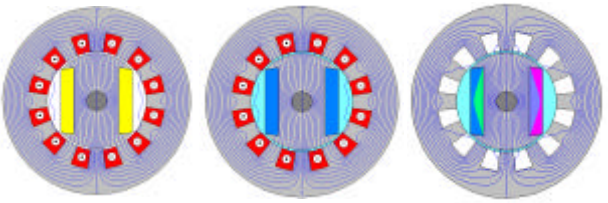

a) Sator switched on, $T>T_c$ b) Sator switched on, $T<T_c$ c) Sator switched off, $T<T_c$

Fig.8 – Sequence of the HTS coil pre-magnetisation

Figure 9 shows a cross section of a HTS synchronous machine, including the cryostat system, with a rated output power of 780 kW, 12000 rpm and 400 Hz. The volume

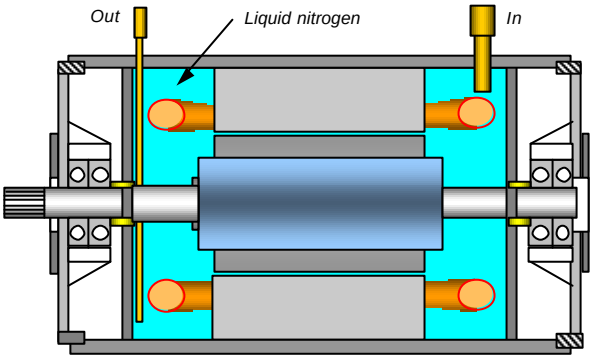

Fig.9 – Cryostat system of the HTS synchronous machine

aspect ratio of this machine compared with a conventional one of the some characteristics is about six times less, giving to this design a near future application in aerospace industry.

6. Theoretical Torque Comparison

Figure 10 shows a comparison of the salient, composite and pre magnetised synchronous torques by the previous machines, relative to the conventional reluctance torque. The theoretical results show that the torque produced by the HTS *salient type motor* is about 1.7 times greater than the torque produced by the conventional motor and the HTS

"Zebra" type, with five iron blocks and six YBCO blocks on the rotor, is about 2.2 times greater, but the construction is more complicated and expensive than that of salient pole.

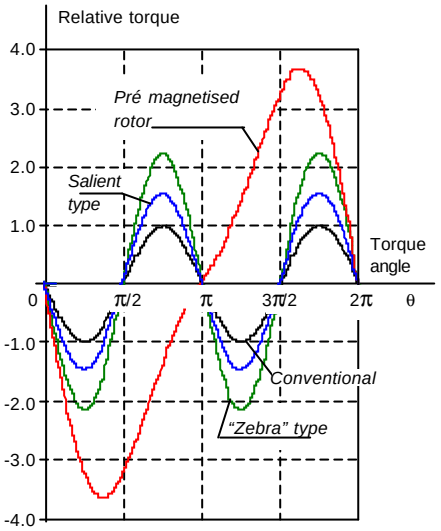

Fig.10 – Relative developed torque comparison

However, the total torque givem by Eq.(1) developed in the *pre-magnetised rotor* is 3.7 times greater than the correspondent conventional reluctance torque.

7. Experimental Results

A powder break was used to measure the output torque and the test rig is shown in figure 11.

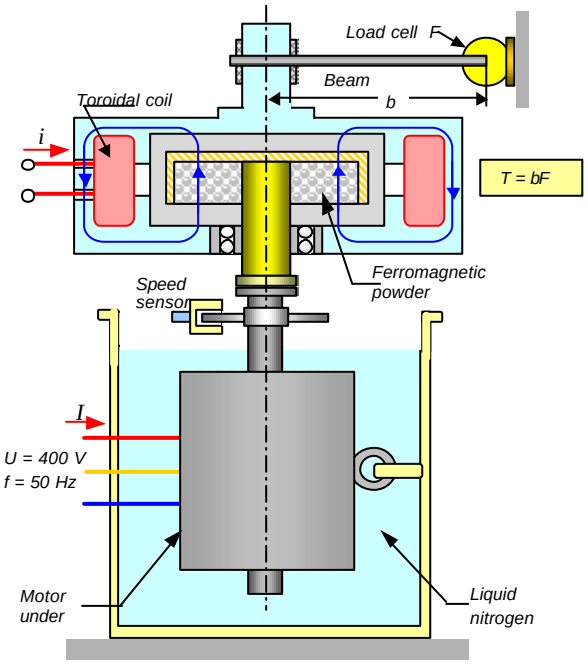

Fig. 11 – Powder break test rig for torque measurement

The previous four rotors were tested using the same conventional two pole three-phase 2 kW stator. By varying the excitation current *i* of the toroidal coil, friction of the ferromagnetic powder generates output motor. Each motor was cooled in a liquid nitrogen container. When the HTS material of the rotor attained the critical temperature, the stator was switched on to 230/400 V, 50 Hz source.

Due to a small rotor cage, the motor has asynchronous/ synchronous self-starting characteristics. Force in the end of a beam of length *b* is measured by means a load cell giving the mechanical torque $T = bF$.

Figure 12a shows experimental results of torque versus input current and figure 12b the power factor for each type of rotor.

For the reluctance motor, the "Zebra" type presents the best torque and power factor. However its construction is a bit more sophisticated. Pre-magnetised synchronous motor presents, obviously, the best characteristics.

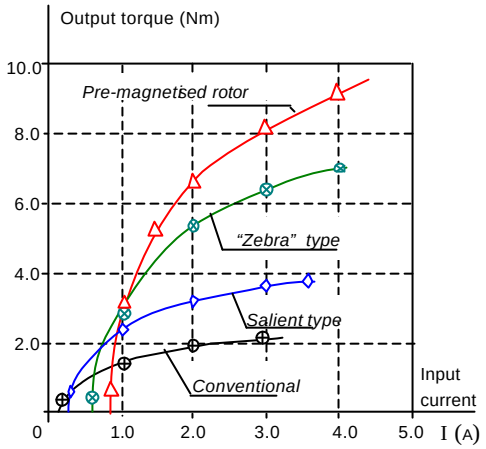

a) Output torque versus stator current.

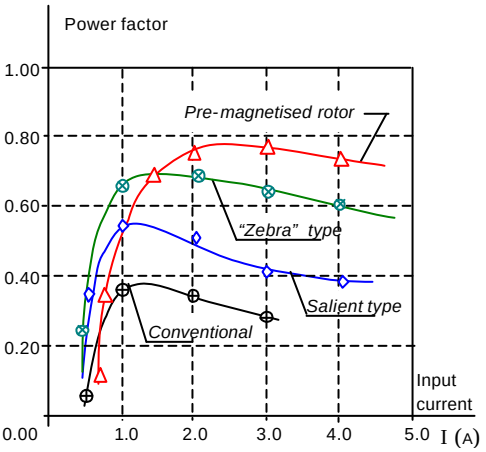

b) Power factor versus stator current.

Fig. 12 – Output torque and power factor versus stator current.

These results agree with the experimental results obtained by Kovalev [10].

8. HTS Hysteresis Motor

When a cylinder of HTS material is placed in a variable magnetic field, superficial currents are induced on the material originating hysteresis losses. The persistent currents on the rotor generate a magnetic flux that reacting with the stator flux produces a electromechanical torque. It can be shown [11] that this torque is proportional to the rotor hysteresis losses, and this is the reason why the device is called hysteresis motor. It is also shown that, contrary to conventional electric motors (e.g. synchronous, asynchronous, hysteresis), the trque of the HTS hysteresis motor results from repulsion of the magnetic poles induced into HTS rotor by the rotating field of the stator winding.

Figure 13a shows the flux distribution in a type-II superconductor cylinder of low critical current density J_c placed in a rotating field and figure 13b a similar cylinder of higher critical current density J_c. Comparison of both plots shows that as the critical current density increases more flux crosses the periphery of the cylinder, leaving the interior inactive.

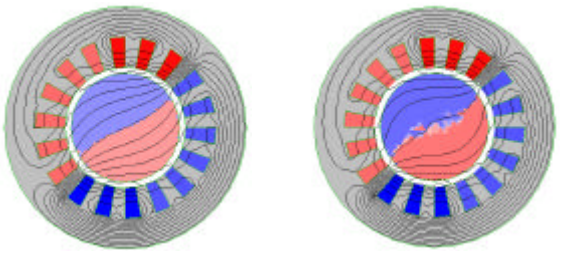

a) Low critical current density b) High critical current density

Fig.13 – Flux penetration in a type-II HTS cylinder

For a HTS cylinder of volume $Vol = (\pi/4)D_o^2\ell$ of diameter D_o and effective length ℓ, placed in a rotating field with an air gap sinusoidal distribution of amplitude $\hat{B}$ reference [9] gives the following torque expression

$$T = \frac{1}{3\pi}\ell D_o^3 J_c \hat{B}\beta(\delta) \quad \text{where} \quad \beta(\delta) = 1 - \frac{1}{\alpha\delta^{2.2}+1}$$

is a dimensionless factor which characterizes the flux penetration. The parameters α and $\delta = (4/\pi)\hat{B}/\mu_o J_c D_o$ depend on the HTS material properties and rotor diameter D_o. For a $2p$ pole hysteresis motor the torque per prismatic rotor volume $D_o^2\ell$ reduces to

$$T_u = \frac{T}{D_o^2\ell} = \frac{p}{3\pi} D_o J_c \hat{B}\beta(\delta) \qquad (3)$$

and increases with rotor diameter.

For HTS materials with small flux penetration, i.e, high J_c, torque can be increased using a ring with a inner diameter D_i. For rotors with this geometry, specific torque expression reduces to

$$T_u = \frac{p}{3\pi} D_o J_c \hat{B}\left[1 - \left(\frac{D_i}{D_o}\right)^3\right]\beta(\delta). \qquad (4)$$

Eq.(4) shows that , as it happens in a conventional hysteresis motor, torque is independent of rotor speed. Computing simulations show that the optimal torque is obtained when $D_i = 0{,}78D_o$, i.e., when the HTS ring width is about 11% of outer rotor diameter. Increasing od D_i generates decreasing of torque, which is obviously zero when $D_i = D_o$.

The configuration of HTS hysteresis machine is shown in figure 14a. The rotor consists of HTS cylindrical elements. Each element can be manufactured as whole cylinder or can be glued from circular sectors in such way that the HTS C axis has the radial orientation. Figure 14b shows the hysteresis motor aspect.

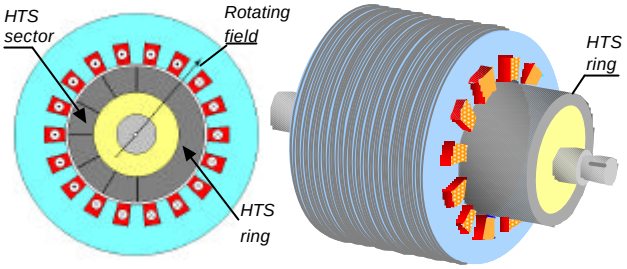

a) Hysteresis motor layout b) HTS motor aspect

Fig. 14 – Hysteresis motor topology

In spite of the HTS brittleness, the rotor constructed in this way is very robust. Figure 15 shows a photograph of a hysteresis rotor constructed with several circular sectors.

Fig. 15 – HYS hysteresis rotor

Figure 16a shows the flux plot for a rotor using four sectors and figure 16b for a rotor using six circular sectors. The plots show that the flux penetration inside the rotor increases with increasing the number of HTS circular sectors due to the epoxy resin between them. Therefore, torque developed will decrease with the number of sectors. Although circular sectors are easier to be produced, the number used in the rotor construction should be limited.

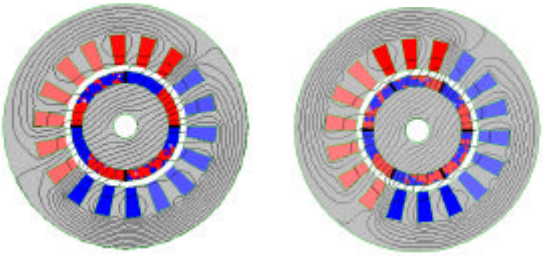

a) Rotor with four sectors b) Rotor with six sectors

Fig. 16 – Flux plot for rotors employing different circular sectors

A hysteresis motor with a single ring of YBaCu rotor with a critical current density of J_c = 3,5x10^7 A/m^2 was tested. For comparison, a conventional hysteresis motor with a large ferromagnetic hysteresis loop was also tested. In figure 17 results of torque per prismatic rotor volume versus stator current density J_S for both type of motors are displayed in the same scale.

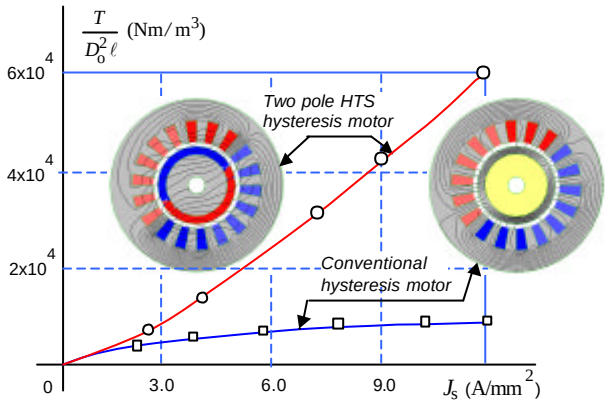

Fig. 17 – Specific torque versus stator current density for conventional and HTS hysteresis motors

Specific torque of HTS hysteresis motor increases almost with the stator current density squared, while for the conventional hysteresis motor is almost constant. The ratio of torque is however of the order of six times.

9. Conclusions

HTS materials are able to change considerably the future power systems in this century because they give the new active materials having unique properties. Compared with conventional motors, HTS motors have specific torque of the order of six times, which makes these devices very powerful machines.

Despite the recent advances in the fabrication of HTS materials, still there exists an inherent difficulty for the construction of single domain pieces suitable for the ring of the HTS hysteresis motor. Thus, it becomes possible to join multiple materials for the rotor fabrication. The finite element modelling of multi-segments machines was utilized to demonstrate the flux and induced current distribution in such motors. Valuable recommendations on the maximization of the torque production could be made.

However, in order to obtain these performances, the rotor must be cooled under the critical temperature of the superconductor. Nevertheless, in locals where installations of liquid nitrogen or liquid hydrogen are available, such as in the near future hydrogen-powered aircrafts (cryoplanes) and other land vehicles, where weight is undesirable, these type of machines can be serious competitors of conventional motors.

Acknowledgement

This work was supported by the RTN Supermachines Project nº HPRN-CT-2000-00036. Thanks are also due to Prof. David Dew-Hughes from Department Engineering Science, University of Oxford, and Prof. Leo Kovalev from Moscow Aviation Institute for the stimulating discussions about HTS motors.

References

[1] J.G. Bednorz and K.A. Müller, "Possible High T_c Superconductivity in the Ba-La-Cu-O System", *Z. Phys.* B, 64 1986.

[2] Department Engineering Science University of Oxford, U.K.; Moscow State Aviation Institute, Moscow, Russia; Institut fuer Physikalische Hochtechnologie, Jena,Germany, Institute de Ciencia de Materials de Barcelona,Bellaterra, Spain; DEE-FCT/UNL, Caparica, Portugal.

[3] M.McCulloch and D.Dew-Hughes: "Brushless ac machines with high temperature superconducting rotors", *Material Science and Engineering B, Elsivier, 1998.*

[4] T.A. Coombs and A.M. Campbell, "A fast algorithm for calculating the critical state in superconductors", *Proc. of the EMF 2000 Conf.*, Ghent, Belgium.

[5] Y.D. Chun, Y.H. Kim, J. Lee, J.P. Hong and Lee.J.W., "Finite element analysis of magnetic field in high temperature bulk superconductor", *IEEE Trans. On Applied Superconductivity*, 11(2001), 2000.

[6] Suguira T, Shashizume H and K Mika, "Numerical electromagnetic field analysis of type II superconductors", *Int J. of Applied Electromagnetics in Materials*, 2(1991), 183.

[7] G. J. Barnes, M. McCulloch, D. Dew-Hughes, "Applications and modelling of bulk HTS in brushless AC machines", *Supercond. Sci. Technology, 13 875-878, 2000.*

[8] G. J. Barnes, D. Dew-Hughes, M. McCulloch, "Torque from hysteresis machines with type II superconducting segmented rotors", *Physica C*, 331(2000), 133-140.

[9] G. J. Barnes, "Computational modelling for type-II superconductivity and the investigation of high temperature superconducting electrical machines", *Ph.D. Thesis, Oxford University, 2000.*

[10]L.K. Kovalev et al: HTS motors design. Recent results and future development" *Superconductivity Research and Development, 1996.*

[11]L.K. Kovalev et al., "Hysteresis and reluctance electric machines with bulk HTS rotor elements", *IEEE Trans. on Applied Superconductivity*, 9(1999), 1261.

* * *